ELSEVIER

Polymer 42 (2001) 7663–7673

polymer

www.elsevier.nl/locate/polymer

Organisation and interactions in aqueous dispersions of polystyrene–polyethylene oxide block copolymer micelles

Gavin J. Brown[a], Randal W. Richards[a,*], Richard K. Heenan[b]

[a]*Department of Chemistry, IRC in Polymer Science and Technology, University of Durham, Durham DH1 3LE, UK*
[b]*ISIS Science Division, Rutherford Appleton Laboratory, Chilton, Didcot, Oxon OX11 0QZ, UK*

Received 22 January 2001; received in revised form 20 March 2001; accepted 26 March 2001

Abstract

Diblock copolymers of polystyrene (PS) and polyethylene oxide (PEO) with a total molecular weight of circa 7500 g mol^{-1} and a PS weight fraction of circa 0.15 have been synthesised in all possible variants of hydrogenous and deuterated forms. The copolymers have been dispersed at concentration above the critical micelle concentration (cmc) in aqueous dispersion mediums of varying contents of light and heavy water to contrast match selected components of the micelles. Small angle neutron scattering has been used to determine the size of the micelles, the radius of the PS core and the thickness of the PEO corona using data for dispersions with concentrations less than or equal to 1×10^{-2} g ml^{-1}. At higher concentrations, a structure factor peak becomes increasingly evident as the concentration increases to 6.5×10^{-2} g ml^{-1}. The total scattering could not be fitted using the structure factor for an assembly of hard spheres; a structure factor originally developed for coulombically stabilised micelles was used and excellent fits to the data obtained. The structure factor is described in terms of a Yukawa potential between the micelles and the values of the repulsion potentials have been used to calculate the repulsive force between the micelles and compared to the predictions for two brush-like polymer layers approaching each other. There is partial agreement with the model, the disagreement being identical to that observed when the results from force balance experiments are compared with the model.

Keywords: Yukawa potential; Polystyrene; Polyethylene

1. Introduction

The most characteristic feature of block copolymers composed of thermodynamically incompatible blocks is the exhibition of microphase separation and the formation of domains of colloidal dimensions in the bulk state [1,2]. These microphase-separated morphologies generally have considerable long-range order and a rich phase behaviour that has been the focus of much activity [1,3–9]. Much of the reported work has been on melts or the bulk solid state of the copolymers with much less attention being paid to their solutions in selective solvents. What has been reported on block copolymer solutions shows that aggregated structures exist in solutions and long-range order develops between them at concentrations significantly less than that of bulk polymer [10–15], the exact concentration depending on the thermodynamics of the interactions between polymer and solvent. Evidently, in dilute solution, micellisation of the copolymer is the forerunner to the microphase separation observed in the bulk state with an ordering process taking place at higher concentrations that may need thermal annealing.

Such micellar structures are of interest as a possible means of obtaining a situation where polymers are attached to a fixed point by one end. Tethered layers have been of fairly constant attention since the first theoretical description of 'brush-like' layers of polymer molecules attached to a solid fluid interface was described by Alexander [16] and de Gennes [17] some 20 years ago. In a copolymer micelle, because the surface of the core is densely populated by the block that is more compatible with the solvent, the distance between these corona chains is small and excluded volume effects between neighbouring overlapping chains lead them to adopting a much more stretched configuration than that for the equivalent polymer in free solution. The nature of this stretched corona layer depends on the ratio of the core radius to the radius of gyration of the corona chain. When the core is large, the segment density distribution can be approximated to that for a polymer tethered to a planar interface, i.e. there will be a parabolic distribution [18]. When the micelle core has a small radius, the configurational

* Corresponding author.
E-mail address: r.w.richards@durham.ac.uk (R.W. Richards).

0032-3861/01/$ - see front matter
PII: S0032-3861(01)00252-X

statistics of the corona chains will be more akin to that of a densely 'armed' star polymer [19]. Much of the attention has focused on the configurational statistics with comparatively little discussion of the structure factor and its repulsion potentials, osmotic compressibilities and pair-distribution functions that are obtainable.

One exception to this is the work of Gast [20–22] who, although primarily interested in the configurational statistics of the corona chains, extracted an intermicellar repulsion potential based on a self-consistent field description of these corona chains and then calculated a liquid like structure factor for concentrated dispersions. This was then compared to the experimentally obtained structure factor from small angle neutron scattering data. There was, however, no fitting of theoretical expressions for the scattering cross-section to the data for the concentrated dispersions of the deutero polystyrene–hydrogenous polyisoprene copolymer investigated.

Diblock copolymers of polystyrene (PS) and polyethylene oxide (PEO) of modest molecular weight form micelles when dispersed in water at concentrations greater than the critical micelle concentration (cmc). For molecular weights in the range from 4000 to ~8000 g mol^{-1}, the cmc is of the order of 10^{-5} g ml^{-1}, the precise value depending on total molecular weight and copolymer composition but with PS always the minority component of the copolymer. Riess et al. [23] used small angle X-ray scattering and quasi-elastic light scattering to investigate dilute (~1% weight per unit volume (w/v)) dispersions of PS–PEO copolymer and determined that for fixed PS content the hydrodynamic radius of the micelle increased as PEO content increased but the core (PS) radius and hence the aggregation number decreased. Mortensen et al. [24] have reported small angle neutron scattering results for a PS–PEO copolymer with block molecular weights of 1000 and 3000 g mol^{-1}, respectively. Only the low concentration data for dispersions in D_2O was fitted and despite the exhaustive nature of the theoretical scattering law used, only the core radius was effectively reported. Radii of gyration of the PEO corona were of only modest values and these seem to us to be at odds with the large distances between micelles that manifests itself as a strong structure factor scattering peak.

In earlier papers, we have discussed the surface organisation of a series of PS–PEO copolymers differing (essentially) only in their locus of deuteration [25]. This isotopic labelling being used to aid the interpretation of the neutron reflectometry data. More recently, we have addressed the capillary wave dynamics of dispersions of these copolymers [26] and have demonstrated that the equilibrium dynamic surface takes circa 15 h to be established. We discuss here the small angle neutron scattering from aqueous dispersions of these copolymers where advantage has been taken of contrast matching to determine the contributions of each component to the single particle form factor, the structure factor and the pair distribution function for dispersions with concentrations from 0.1 to 6.5% w/v (in one case). We outline the theoretical background to small angle neutron scattering and the relation between structure factors, pair distribution functions and interparticle potential energy functions.

2. Theoretical background

The small angle neutron scattering cross-section after subtraction of background scattering is given by

$$\frac{d\Sigma(Q)}{d\Omega} = P(Q)S(Q)N_p V_p^2(\rho_p - \rho_m)^2 \quad (1)$$

N_p is the number of scattering particles per unit volume, each of which has a volume V_p. The scattering length density of the particle is ρ_p whilst that of the medium surrounding it is ρ_m. The actual 'shape' of the scattering as a function of scattering vector, Q ($=(4\pi/\lambda)\sin\theta$ for incident wavelength λ and scattering angle 2θ) is determined by the convolution of the particle form factor, $P(Q)$, with the structure factor, $S(Q)$. The latter arises from long-range correlations between scattering particles and in the limit of the bulk state can have the features of crystalline diffraction. When the scattering system is sufficiently dilute or there is no long range ordering between the scattering particles, $S(Q) = 1$ and the features of the scattering are determined by $P(Q)$. Particle form factor expressions have been derived for many different particle shapes with regular and irregular geometry, e.g. solid spheres and hyperbranched polymers [27,28] particular relevance to the micellar scattering entities discussed here is the single particle form factor for a core-shell particle, the details of which are given in Fig. 1. In this case, to account for the different scattering length densities of core, shell and medium Eq. (1) is rewritten in a slightly different form

$$\frac{d\Sigma(Q)}{d\Omega} = \frac{16\pi^2}{9} N_p P(Q)S(Q) \quad (2)$$

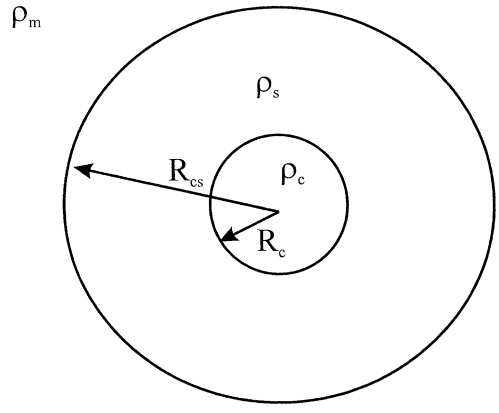

Fig. 1. Schematic diagram of a core shell particle with the radii and scattering length densities in Eq. (3) shown.

and [29]

$$P(Q) = (\rho_s - \rho_m)^2 R_{cs}^6 P(Q, R_{cs}) + 2(\rho_s - \rho_m)(\rho_c - \rho_s) R_c^3 R_{cs}^3 P(Q, R_c)^{1/2} P(Q, R_{cs})^{1/2} + (\rho_c - \rho_s)^2 R_c^6 P(Q, R_c) \quad (3)$$

and $P(Q, R_i)$ is the single particle form factor for a sphere of radius R_i, i.e.

$$P(Q, R_i) = \left[3 \frac{(\sin(QR_i) - QR_i \cos(QR_i))}{(QR_i)^3} \right]^2$$

Consequently, if the isotopic labelling can be manipulated such that $\rho_s = \rho_m$, then the scattering is that from the core alone. When $\rho_c = \rho_m$, the scattering is that of a spherical shell of thickness $R_s = (R_{cs} - R_c)$.

Short-range correlations between fluid particles are expressed numerically by the pair distribution function $g(r)$ [30,31], and the interference function is the Fourier transform of $g(r)$, i.e.

$$S(Q) = 1 + 4\pi N \int_0^{00} (g(r) - 1) \frac{\sin(Qr)}{Qr} r^2 \, dr \quad (4)$$

and $g(r)$ is related to the potential of mean force between the fluid particles. Exact expressions for $S(Q)$ can be obtained for hard sphere fluids from Percus–Yevick theory [32,33] and in terms of the dimensionless quantity $2RQ$, ($R =$ particle radius) for spherical particles with a hard sphere repulsion potential

$$S(2QR) = \frac{1}{1 + 24\eta G(2QR)/2QR} \quad (5)$$

$\eta =$ volume fraction of hard spheres

$$G(x) = \frac{\alpha}{x^2}(\sin x - x\cos x) + \frac{\beta}{x^3}(2x \sin x + (2 - x^2)\cos x - 2) + \frac{\gamma}{x^5}(-x^4 \cos x + 4[(3x^2 - 6)\cos x + (x^3 - 6x)\sin x + 6] \quad (6)$$

and the factors α, β and γ are functions of the hard sphere volume fraction. In common with many relations between $g(r)$ and the interparticle potential, $u(r)$, this Percus–Yevick result is an approximation because one of the integral expressions in the solution of the Ornstein–Zernike [34] relation is an infinite series. All the closed solutions proposed are thus approximations and consequently may produce inconsistent results when other properties are calculated from $g(r)$. Nonetheless, hard sphere potentials have been used with some success to reproduce the scattered intensity from disordered block copolymers in the solid state [35] and dispersions of latex particles both Coulombically and sterically stabilised [29,36]. It is a modification of this Percus–Yevick description that we have used in the analysis of our scattering data.

3. Experimental

3.1. Diblock copolymers

Anionic synthesis was used to prepare diblock copolymers of styrene and ethylene oxide using the method of Jialanella et al. [37]. Four isotopic variants were synthesised to explore the maximum small-angle neutron scattering contrast, these were; both blocks deuterated (dPS–dPEO), both blocks hydrogenous (hPS–hPEO) and the remaining two copolymers having one hydrogenous and one deuterated block, hPS–dPEO and dPS–hPEO. Each of these were synthesised with as close an agreement between them as possible in terms of molecular weight and composition. Molecular weights were obtained by SEC using chloroform as the eluting solvent and compositions obtained from solution state ^{13}C NMR, these data are given in Table 1.

3.2. Dispersion preparation and small-angle neutron scattering

Aqueous dispersions of each copolymer were prepared by mixing the copolymer with the appropriate dispersion medium (see below), heating to 333 K and then allowing to cool to room temperature. The dispersion medium for each copolymer was chosen to provide maximum contrast with either the whole copolymer or for individual components. Hence for the former, hPS–hPEO was dispersed in heavy water and dPS–dPEO dispersed in a mixture of heavy and light water with a net scattering length density of zero. SANS from the PS component alone was obtained by dispersing the dPS–hPEO copolymer in that mixture of the two isotopic variants for water that produced a scattering length density equal to that of hPEO. In a similar manner the hPS–dPEO copolymer was used to obtain the SANS due to the PEO component alone.

SANS data were obtained using the LOQ diffractometer at the UK pulsed neutron source ISIS, Rutherford Appleton Laboratory, Didcot, UK. Each dispersion was placed in quartz cells of 1 mm path length that were maintained at 298 K whilst the data were collected. In all cases the scattering was radially isotropic about the beam direction, consequently the counts of the two-dimensional detector were radially averaged. After correction for transmission and subtraction of the dispersion medium scattering, the

Table 1
Molecular weights and compositions of copolymers

Copolymer	Molecular weight PS block (g mol^{-1})	Copolymer molecular weight (g mol^{-1})	Mole fraction PS	Weight fraction PS
dPS–dPEO	1280	7580	0.072	0.15_3
dPS–hPEO	1280	6670	0.074	0.16_9
hPS–dPEO	1430	8180	0.070	0.14_0
hPS–hPEO	1430	8490	0.077	0.16_4

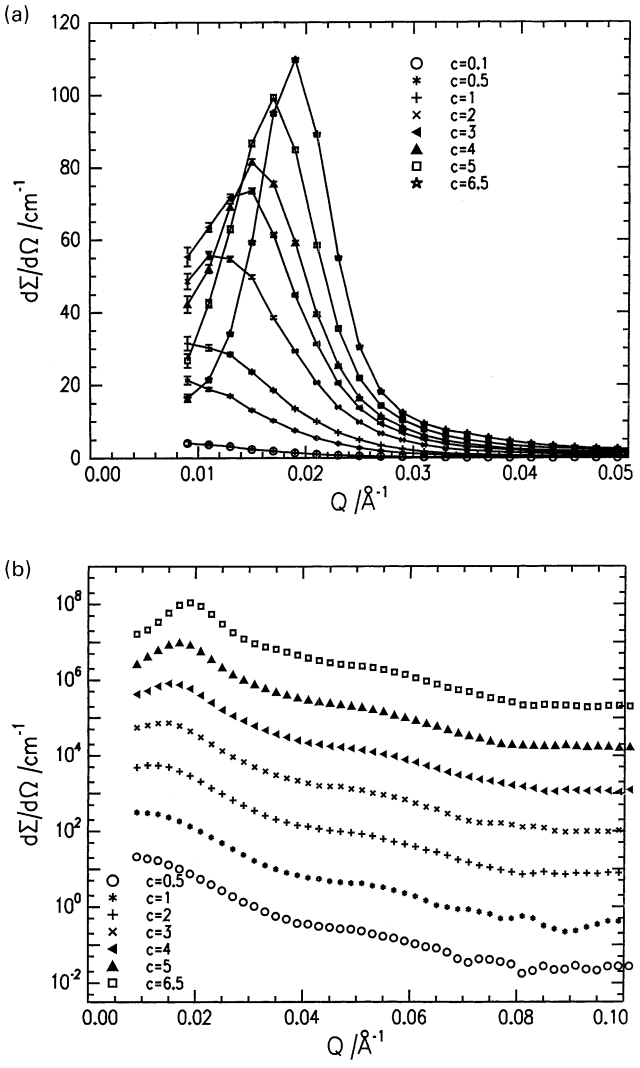

Fig. 2. (a) Scattering cross-sections for all concentrations of the hydrogenous copolymer dispersed in D_2O. Lines are guides for the eye. (b) Semi-logarithmic plot of the same data, each data set has been translated vertically by one decade from the preceding concentration data set. Concentrations are given in units of 10^{-2} g ml^{-1}.

data were converted to absolute scattering cross-sections ($d\Sigma/d\Omega$ cm) by comparison to the $Q = 0$ scattering for a well characterised blend of hydrogenous and deuterated PS. The range of block copolymer concentrations explored was from 5×10^{-4} to 6.5×10^{-2} g ml^{-1}, all contrasts were explored for dispersion concentrations up to 5×10^{-2} g ml^{-1} inclusive. For concentrations of 6×10^{-2} and 6.5×10^{-2} g ml^{-1}, SANS data for hydrogenous dispersions in D_2O only were collected. Concentrations above 6.5×10^{-2} g ml^{-1} were intractable, rigid gel-like materials being formed and the distribution of the aqueous phase was evidently inhomogeneous on visual inspection. The Q range utilised was $9 \times 10^{-3} \leq Q$ (Å^{-1}) ≤ 0.2, however the scattering had decayed to background levels ($\simeq 0$ after subtraction of dispersion medium scattering) and consequently data presented here are confined to scattering vectors no higher than 0.1 Å^{-1}.

4. Results and discussion

In Fig. 2, we show the scattering profiles for the complete range of concentrations of the hydrogenous copolymer dispersed in D_2O. On this linear–linear scale, the scattered intensities for $Q > 0.05$ Å^{-1} are very small and indistinguishable from each other. Evidently, the nature of the scattering changes between concentrations of 1×10^{-2} and 2×10^{-2} g ml^{-1}. For the latter concentration the maximum intensity is twice that for the 1×10^{-2} g ml^{-1} dispersion and moreover a maximum is evident. This structure factor maximum increases in amplitude and shifts to larger Q values as the concentration increases. For concentrations of 4×10^{-2} g ml^{-1} and above, the structure factor scattering is dominant. When the data are plotted in the semi-logarithmic form of Fig. 2b the contribution of the single particle form factor becomes evident with second order maximum centred at $Q \simeq 0.052$ Å^{-1}. This contribution to the scattering profile is clearly evident in the data for the dPS–hPEO copolymers dispersed in hPEO contrast matching water (Fig. 3). At concentrations of 1×10^{-2} g ml^{-1} and below only the single particle form factor scattering is evident, structure factor scattering is noted for concentrations of 2×10^{-2} g ml^{-1} and greater. The absence of a series of well-defined maxima arising from the structure factor scattering suggests that although there is long-range order in the dispersions as shown by the strong maximum in the intensity, the micelles are not arranged in a highly organised manner. However, inspection of the scattering data shows the presence of a second maximum (albeit broad and weak) at a Q value approximately twice that for the first structure factor maximum. A second structure factor maximum is not evident in the scattering from the hPS–dPEO dispersions, the intensity of scattering decreasing rapidly after the structure factor maximum is passed.

4.1. Single particle form factor and micelle dimensions

Double logarithmic plots of the SANS data for the dilute dispersions (i.e. concentrations $\leq 1 \times 10^{-2}$ g ml^{-1}) reveal no Q exponents of -1 indicative of cylindrical micelles being present. Furthermore, shear experiments on these dispersions showed no evidence of preferred alignment, hence we conclude that the micelles are spherical in nature. Approximate values for the micelle dimensions can be obtained from the limiting slope as Q approaches zero of Guinier plots ($\ln(d\Sigma(Q)/d\Omega)$ as a function of Q^2). Data for dispersions with concentrations of 0.5×10^{-2} g ml^{-1} are shown in Fig. 4 and the radii of the equivalent spheres are 56 Å for the dPS core, 183 Å for case where the core is contrast matched and 135 Å for the hydrogenous copolymer dispersed in D_2O. These values suggest that the PEO corona has a thickness of circa 125 Å. The difference in radii between the core contrast and hydrogenous polymer in D_2O is due to the different weightings given by the contrast factors to the individual form factors in Eq. (3) and small

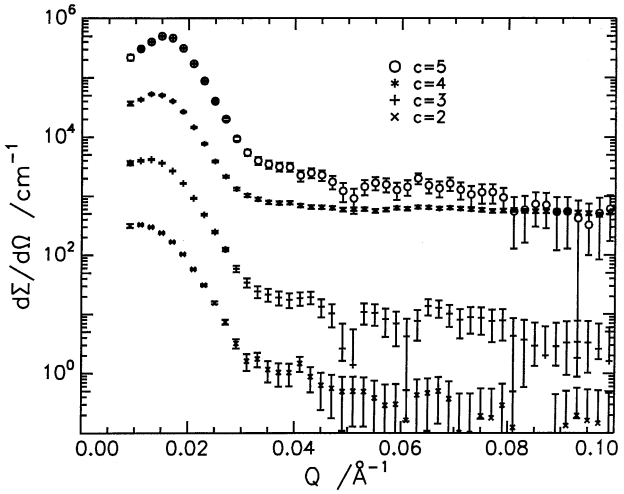

Fig. 3. Semi-logarithmic plot of scattering cross-section for hPS–dPEO diblock copolymer dispersed in water contrast matched to hPS. Each data set is translated vertically by one decade from that of the preceding concentration. Concentrations are given in units of 10^{-2} g ml^{-1}.

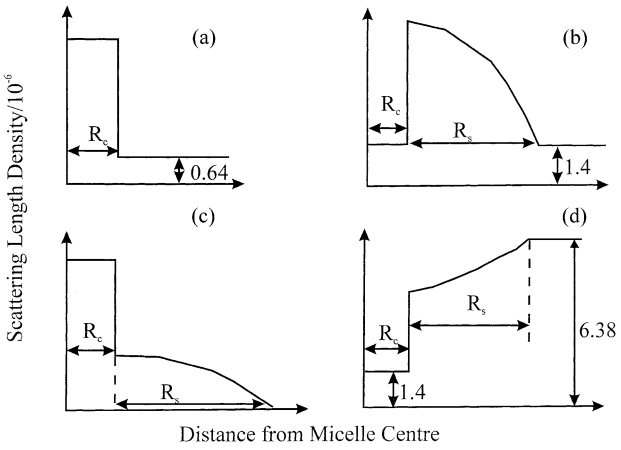

Fig. 5. Schematic drawings of the scattering length density distributions used in fitting to the single particle form factor scattering of the dilute dispersions. (A) dPS–hPEO in water contrast matched to hPEO, (B) hPS–dPEO in water contrast matched to hPS, (C) dPS–dPEO in water with zero scattering length density, (D) hPs–hPEO in deuterium oxide. Units of scattering length density are Å^{-2} and pertinent values are indicated on each diagram.

differences in the molecular weights of the different isotopically labelled copolymers. The average radius of gyration for PEO with the molecular weight of the block in these copolymers is 27 Å [38], hence the blocks in the corona are highly stretched.

To obtain more accurate values of core and corona dimensions, the scattering cross-section was calculated for a model of the micelle where a variation in the monomer density in the corona was allowed for. The core of the micelle was assumed to contain only PS and to be of uniform density. The distribution of PEO in the corona was modelled by a series six linear segments corresponding to the local volume fraction of PEO. Fig. 5 sketches the variation in scattering length density for each neutron scattering contrast condition used. In fitting this adjusted core-shell model to the scattering cross-section data, the adjustable parameters were R_c, R_s, and the differences in scattering length density at core–corona interface $\Delta\rho_c$ and over the corona thickness, $\Delta\rho_s$. Additionally, polydispersity in micelle size was allowed for by incorporating a Schultz distribution in the core radius. Fig. 6 shows examples of the fits obtained using dispersions where the concentration was 1×10^{-2} g ml^{-1}. Table 2 gives the values of $\bar{R}_c$, R_s, $\Delta\rho_c$, $\Delta\rho_s$, and $\sigma/\bar{R}_c$ where σ is the standard deviation of the Schultz distribution. The average mean core radius was 45 Å and the average corona thickness was 132 Å. The average value of $\sigma/\bar{R}_c$, 0.27, corresponds to a weight average micelle radius to number average radius of less than 1.1. The aggregation number of the micelle, i.e. number of copolymer molecules per micelle is given by

$$\bar{N}_{ag} = \frac{\text{Micelle core volume}}{\text{Volume occupied by PS block}}$$

and using a mean PS block molecular weight of 1355 g mol^{-1}, there are 170 copolymer molecules in each micelle. The distance between each PEO block on the surface of the PS core is $(4\pi\bar{R}_c^2/\bar{N}_{ag})^{1/2}$, and a value of 12 Å results. This separation distance is far smaller than the radius of gyration of the PEO block and consequently supports the notion of the block being highly stretched as observed in the corona thickness being almost five times the radius of gyration of the PEO block. Also included in Table 2 are values of the volume fraction of water in the corona of the micelle calculated at the boundary between the core and corona using the values of scattering length density on the presumption that the corona is composed of only PEO and water.

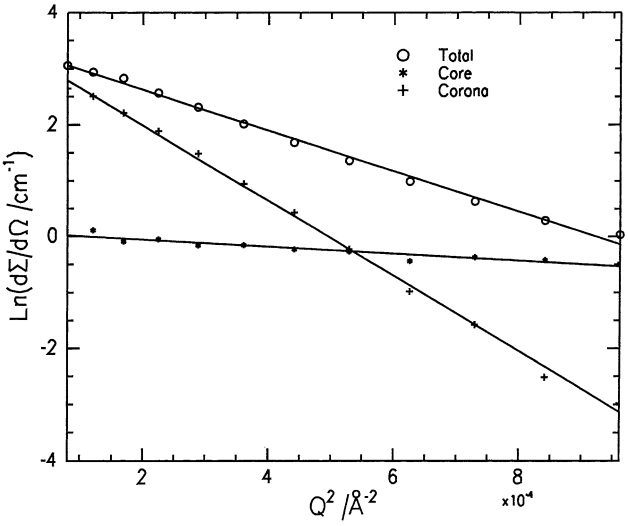

Fig. 4. Guinier plots for the diblock copolymers dispersed in water at a concentration of 0.5×10^{-2} g ml^{-1}. Total is for hPS–hPEO in D_2O; core is for dPS–hPEO in water contrast matched to hPEO; corona is for hPS–dPEO in water contrast matched to hPS.

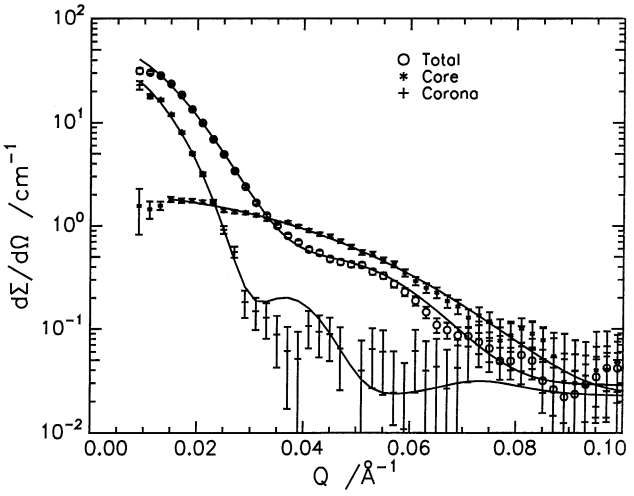

Fig. 6. Fits of particle form factor to scattering data for hPS–hPEO in D_2O (total), dPS–hEO in water contrast matched to hEO (core) and hPS–dEO in water contrast matched to hS (corona). All the data are for a copolymer concentration of 1×10^{-2} g ml^{-1}.

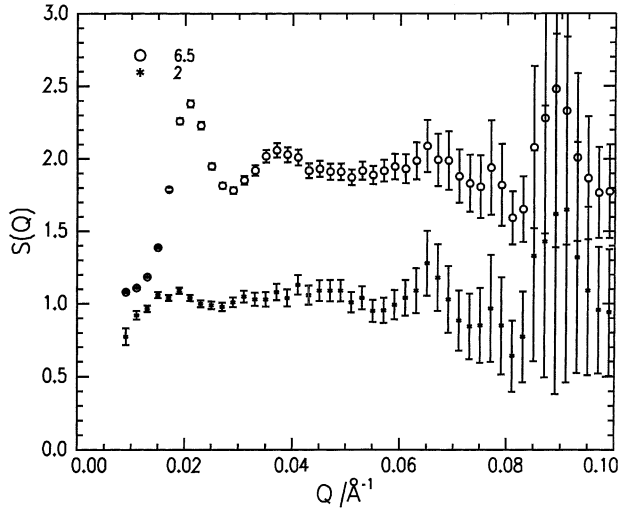

Fig. 7. Structure factors obtained via Eq. (8) for hPS–hPEO dispersed in D_2O at the concentrations indicated in units of 10^{-2} g ml^{-1}. The 6.5×10^{-2} g ml^{-1} dispersion data has been translated vertically by 1 for clarity.

4.2. Structure factor and pair distribution function

Writing Eq. (1) for a dilute dispersion, where $S(Q) = 1$, and for a concentrated dispersion where $S(Q)$ has finite deviations from 1, and for the same contrast conditions we have

$$\left(\frac{d\Sigma(Q)}{d\Omega}\right)_{dil} = N_{Pdil} V_p^2 (\rho_p - \rho_m)^2 P(Q)$$

$$\left(\frac{d\Sigma(Q)}{d\Omega}\right)_{con} = N_{Pcon} V_p^2 (\rho_p - \rho_m)^2 P(Q) S(Q) \quad (7)$$

Hence, presuming there is no change in the size of the micelles with increasing concentration then

$$S(Q) = \left[\left(\frac{d\Sigma(Q)}{d\Omega}\right)_{con} / \left(\frac{d\Sigma(Q)}{d\Omega}\right)_{dil}\right] \frac{N_{Pdil}}{N_{Pcon}}$$

Fig. 7 shows the results of this division and correction for concentration differences for hydrogenous dispersions at concentrations of 2×10^{-2} and 6.5×10^{-2} g ml^{-1} in D_2O. Evidently, a structure factor is obtained and that oscillates about a value of unity indicating that the calculation of Eq. (7) is approximately correct. However, the procedure is sensitive to a number of factors. Firstly, the availability of precise concentrations of the dilute and concentrated dispersions for correct normalisation. Secondly, statistical deviations in scattering cross-sections for the dilute dispersions at high Q values may change $S(Q)$ values. Thirdly, propagation of two sets of errors in the cross-section data can lead to unacceptably large uncertainties in $S(Q)$.

Consequently, to obtain the partial structure factor we have fitted the scattering cross-section data for dispersions with concentrations $\geq 2 \times 10^{-2}$ g ml^{-1} using Eq. (1), i.e. the convolution of form factor and structure factor. To simplify the computation the simple core-shell model was used,

Table 2
Parameters of PS–PEO micelles obtained from fitting adjusted core-shell model to scattering cross-section data

Copolymer	c (10^{-2} g ml^{-1})	$\bar{R}_c$ (Å)	R_s (Å)	$\Delta\rho_c$ (10^{-6}Å^{-2})	$\Delta\rho_s$ (10^{-6}Å^{-2})	$\sigma/\bar{R}_c$	ϕ_w
dPS–dPEO	1	43	127	5.5	0.97	0.3	0.86
	0.1	46	124	5.14	1.32	0.3	0.0.81
	0.05	43	139	5.55	0.92	0.3	0.87
hPS–hPEO	1	47	125	4.24	0.73	0.3	0.87
	0.1	46	128	4.3	0.68	0.3	0.88
	0.05	46	131	4.3	0.67	0.3	0.88
dPS–hPEO	1	43	–	5.8	–	0.14	–
	0.1	47	–	5.8	–	0.2	–
	0.05	43	–	5.8	–	0.3	–
hPS–dPEO	1	43	133	0.8	0.8	0.2	0.86
	0.1	47	139	0.8	0.8	0.22	0.86
	0.05	45	141	0.8	0.8	0.3	0.86

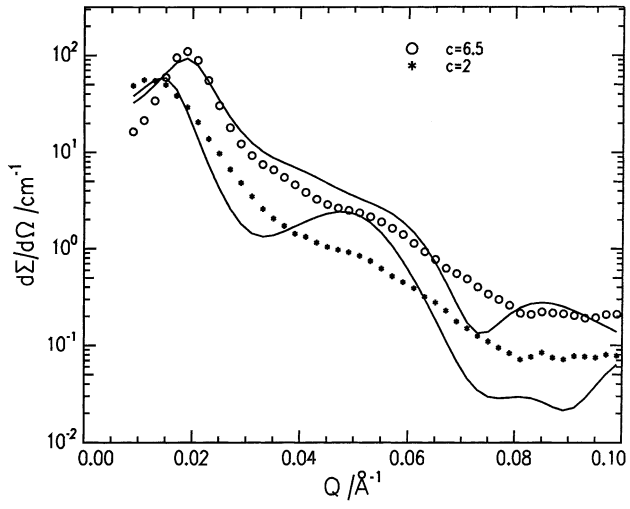

Fig. 8. Best fits obtained using the hard sphere form of $S(Q)$ in fitting to the data for dispersions with concentration (in units of 10^{-2} g ml^{-1}). In this semi-logarithmic scale the error bars are within the data points. The parameters for each fit are; 6.5×10^{-2} g ml^{-1} core radius 60 Å, corona thickness 92 Å and micelle number density 1.96×10^{-6} Å^{-3}; 2.0×10^{-2} g ml^{-1} core radius 52 Å, corona thickness 127 Å and micelle number density 8.63×10^{-7} Å^{-3}.

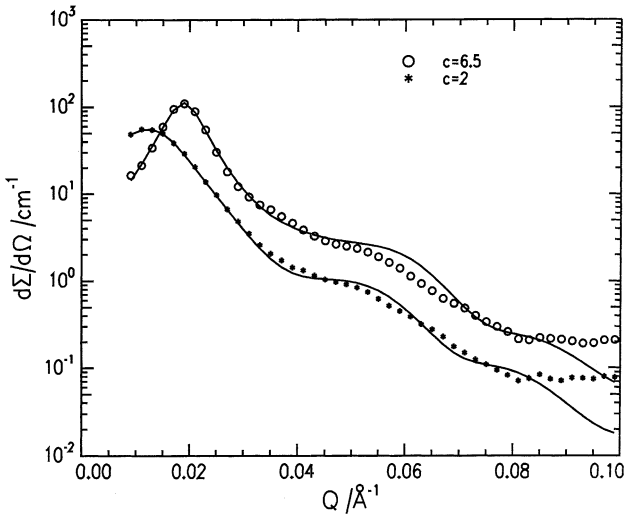

Fig. 9. Fits obtained to the same data sets as in Fig. 8 but using a Yukawa potential and the mean spherical approximation for $S(Q)$.

i.e. we made no allowance for a density distribution of ethylene oxide segments in the micelle corona. Initially, a hard sphere expression for $S(Q)$ (Eq. (5)) was used, however the best non-linear least squares fit of this combination to the data was extremely poor as Fig. 8 shows, and this was especially true for the dispersion with the lowest concentration. We have therefore, used a form of $S(Q)$ that has a more flexible Yukawa potential and uses the mean spherical approximation as the closure for the pair distribution function [39–41]. The Yukawa potential has a 'soft' tail at large separations of the particles, the repulsion potential becoming hard sphere-like at short distances between them. In dimensionless units the potential is given by

$$\beta^{-1}U(x) = \gamma\exp(-kx)/x \qquad x = r/D,\ \ k = \kappa D,\ \ \beta = k_{\mathrm{B}}T \tag{8}$$

where γ is a dimensionless coupling constant and κ is a reciprocal screening length for particles of diameter D. In the non-linear least squares fitting of this combination of $P(Q)$ and $S(Q)$, the parameters that were allowed to vary were the radius of a now monodisperse core, the corona thickness, the scattering length density of the corona (presumed to be uniform over the total corona thickness), the number density of micelles, the coupling constant γ and the dimensionless reciprocal screening length, k. Examples of the fits to the same data sets as used in Fig. 8 are shown in Fig. 9 and are much improved over those obtained using a simple hard sphere potential. Table 3 sets out the values obtained for the hydrogenous copolymer dispersed in D_2O. The PS core radii obtained are marginally larger than those given in Table 2 obtained by using the more sophisticated form factor and scattering data for dilute dispersions. There is a large difference in the corona thicknesses reported in Tables 2 and 3, the much smaller values in Table 3 are attributable to the uniform density corona used in the form factor to fit the scattering from the concentrated dispersions. The number density of micelles in Table 3 scale to each other roughly in proportion to the concentration of each dispersion, absolute values of the copolymer concentration are incorporated in Table 3. Using the average number of copolymer molecules per micelle obtained from the dilute dispersion data in conjunction with the number density of micelles from the fit produces concentrations that are somewhat smaller than that actually used. If the aggregation number is calculated from the value of R_c obtained in fitting the total scattering, then the concentrations calculated are larger than those given in Table 3. From the scattering length density of the corona obtained in the fit, the corona has a volume fraction of water of 0.92 of the same order of magnitude as the values given in Table 2. There appears to be no correlation of values of γ and k with the dispersion concentration, however in the calculation of the structure factor these two parameters are always coupled in the expression for the repulsion potential. The product $\gamma\exp(-k)$ generally shows a decrease with decreasing concentration of the dispersion.

The total micellar radius, $\bar{R}_c$ plus R_s from Table 3 was used together with n and the values of γ and k to calculate the structure factor using the mean spherical approximation and the Yukawa closure as incorporated into the expressions for the structure factor set out in Appendix A. Fig. 10a presents all the structure factors for the hPS–hPEO dispersions in D_2O. As the concentration increases the oscillations around unity become more prominent and persist to larger values of QD symptomatic of increased correlations between the micelles, the position of the first maximum shifts to larger values of QD. Both of these aspects are made more apparent in Fig. 10b where the calculated

Table 3
Parameters obtained by fitting convoluted form factor and structure factor to scattering cross-section data of hPS–hPEO in D_2O

	c (10^{-2} g ml^{-1})					
	6.5	6	5	4	3	2
$\bar{R}_c$ (Å)	52	52	53	53	55	54
R_s (Å)	94	94	96	96	99	97
ρ_s (10^{-6}Å^{-2})	5.9	5.9	5.9	5.8	5.8	5.8
n (10^{-8}Å^3)	2.23	2.10	1.63	1.18	0.86	0.57
γ	25	23.6	25.8	522.3	4774.0	388.4
K	1.6	1.9	2.3	5.6	8.1	5.4
$\gamma \exp(-k)$	5.1	3.6	2.6	1.9	1.4	1.8
c (10^{-2} g ml^{-1}) calculated	5.75	5.42	4.2	3.04	2.2	1.47

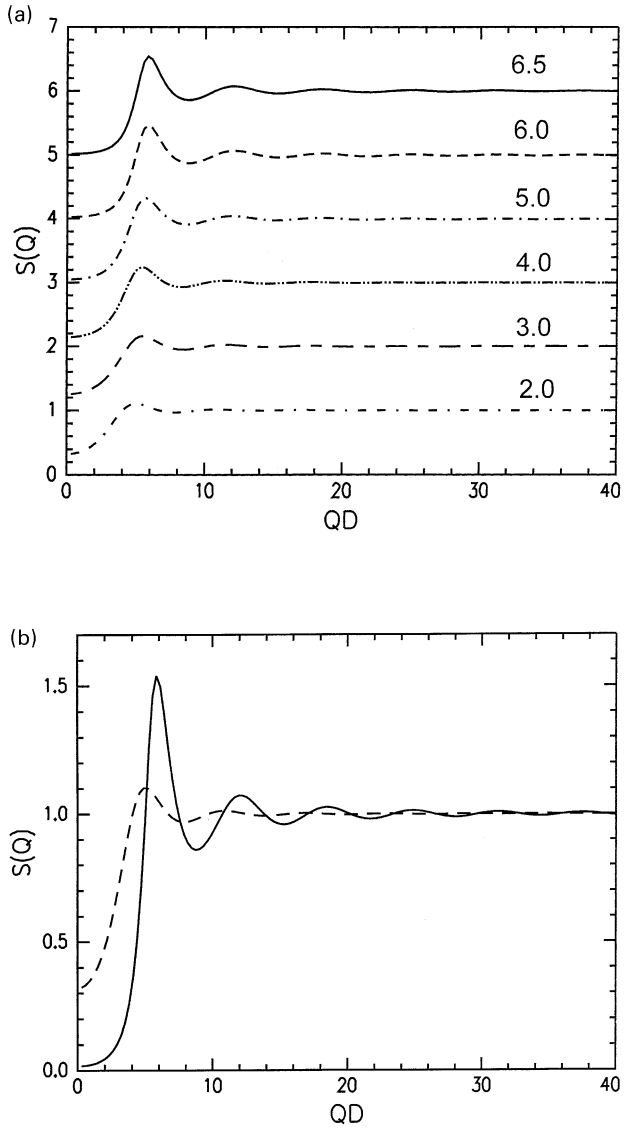

Fig. 10. (a) Structure factors obtained using a Yukawa potential for all concentrations of hPS–dPEO in D_2O $\geq 2 \times 10^{-2}$ g ml^{-1}. Each structure factor is shifted by unity from that of the preceding lower concentration dispersion. Concentration (10^{-2} g ml^{-1}) marked on each set. (b) Overlay of structure factors for concentration 2×10^{-2} g ml^{-1} (– – –) and 6.5×10^{-2} g ml^{-1} (—).

structure factors for concentrations of 2×10^{-2} and 6.5×10^{-2} g ml^{-1} are overlaid with each other, we note that the maximum value of $S(Q)$ is of the same order of magnitude as observed for sterically stabilised PS latex particles but significantly smaller than noted for similar particles that were coulombically stabilised [29]. At $QD = 0$, the structure factor is related to the osmotic compressibility of the dispersion; $(d\pi/dn)_T$ and $(d\pi/dn)_T = k_B T/S(O)$.

Fig. 11 shows the dependence of this osmotic compressibility on the number density of micelles.

The dominant structure factor peak in the scattering intensity notwithstanding, there is in fact little long range ordering beyond nearest neighbour micelles in these dispersions, even at the highest concentration used which is just below the point where the dispersions become an intractable gel. This is demonstrated by the pair distribution functions, $g(r)$ (Fig. 12), obtained by Fourier transforming the $S(Q)$ data. There is essentially no correlation between micelles separated by more than four times their diameter because the pair distribution essentially has a value of unity. For the lowest concentration dispersion where a structure factor is evident in the scattering (2% w/v), only three micelle diameters are required before $g(r)$ has a value of 1.

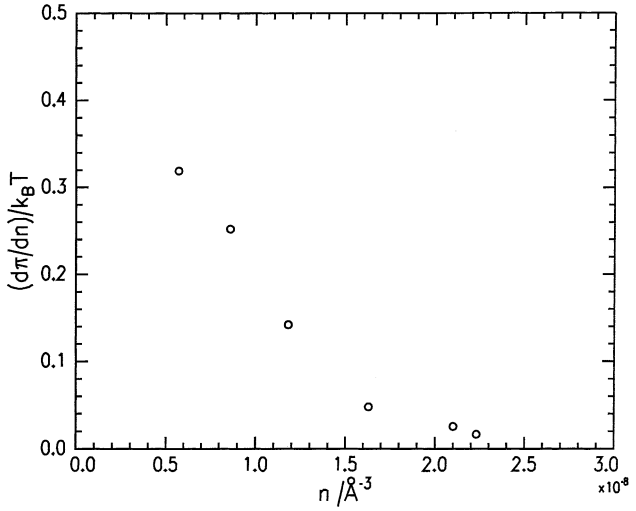

Fig. 11. Osmotic compressibilities as a function of micelle number density for hPS–hPEO in D_2O.

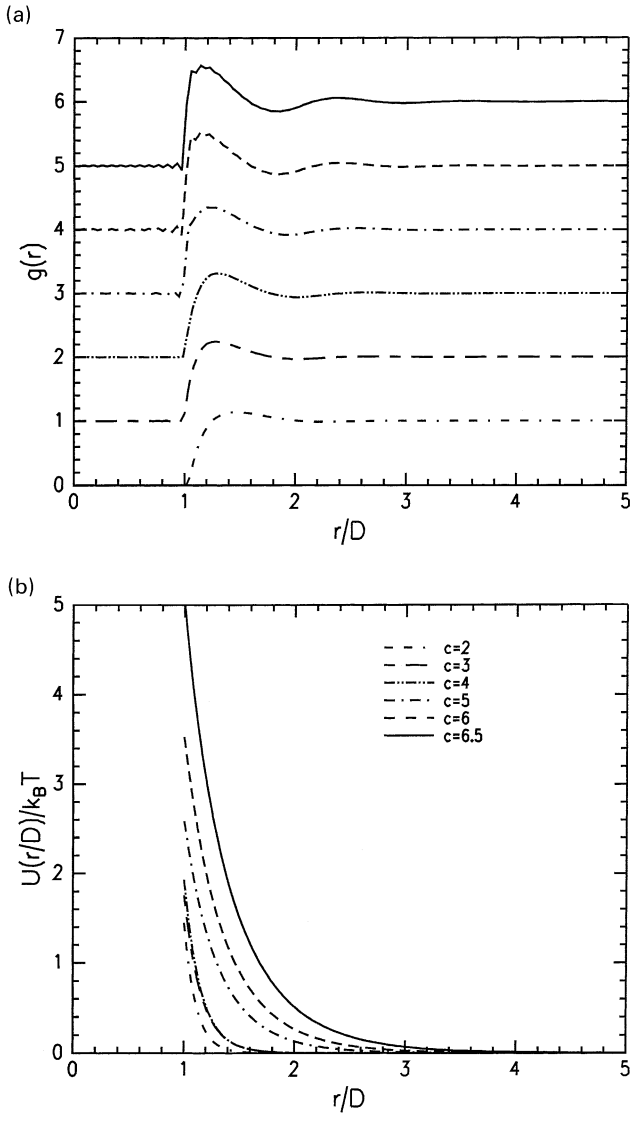

Fig. 12. Pair distribution functions obtained for hPS–dPEO in D_2O. Each curve is displaced upwards by one from the preceding curve and are in the same order as Fig. 10a. (b) Repulsion potentials associated with the pair distribution functions in (a). Concentrations of the dispersions in units of 10^{-2} g ml^{-1} are; solid line 6.5; dashed line 6; dot–dash line 5; dash–two dots line 4; short dash–long dash 3; two dashes–dot line 2.

The repulsion potentials were calculated from Eq. (8) using the values of γ and k from the fits to the scattering data and are plotted in Fig. 12b as a function of the dimensionless separation, r/D, between the micelles. For dispersion concentrations between 2×10^{-2} and 4×10^{-2} g ml^{-1}, the repulsion potentials are essentially identical and become finite at separations just greater than the micelle diameter. The magnitude of the potential is small and only reaches a value of k_BT when the separation distance is one micelle diameter. For these concentrations there must be considerable thermally induced stochastic fluctuations in the equilibrium separation of the micelles. Repulsion between the micelles becomes evident at greater separations for dispersions with higher concentrations and rises more rapidly to much larger values. The potentials are hard sphere like at values of r/D approaching one but have a soft tail at longer distances as anticipated from the form of the potential function used. Both the magnitude and the form of these potential functions are very similar to those derived by McConnell et al. [21,22] from self-consistent field calculations on the segment density distribution in block copolymer micelles.

The repulsion potential has two contributing components, one arising from the osmotic free energy of the brush-like layer of the corona tending to swell the layer by excluded volume effects, the second being the elastic free energy that resists stretching of the corona blocks. Both of these aspects have been explicitly incorporated into an expression relating the force developed between two brush-like layers as they approach each other [42]. A comparison of the predictions of this description has been made to experimental data obtained for brush layers of PS and polyisoprene using a surface forces apparatus [43]. There is an empirical osmotic correction parameter in the expression and agreement between theory and experiment can be obtained by small adjustments in the value of this parameter. Apart from this factor the expressions defined by Patel et al include the grafting density, the excluded volume exponent for the brush polymer in solution, the segment length and a proportionality factor in the power law relating solution osmotic pressure to the concentration of polymer in solution. Evidently, the value of some of these parameters will be unique to the polymer–solvent combination at issue (e.g. segment length and the osmotic proportionality factor) and certainly the proportionality factor does not appear to be available for PEO in water. However, in the excluded volume limit, these factors will probably not vary widely as the polymer-solvent combination changes. The dependence of the repulsive force developed on the separation is presented as plots of reduced force, f, as a function of reduced distance, δ, where

$$f = \frac{\text{Force}}{(\sigma^{(2\upsilon+1)/2\upsilon} b^{1/\upsilon} N)}$$

$$\delta = \frac{r}{(2\sigma^{(1-\upsilon)/2\upsilon} b^{1/\upsilon} N)}$$

We have used the Derjaguin [44] approximation to calculate the force per unit area due to the repulsion potential between micelles, i.e.

$$F(r/D) = \pi R_c U(r/D)$$

where we have retained the dimensionless distance scale in expressing both the force and potential function. Using the parameters obtained for the Yukawa potential from fitting to the scattering from the high concentration dispersions, the dimensionless force obtained is compared to the predictions of the theory of Patel et al. in Fig. 13. The shapes of the two curves are very similar over the same ranges of reduced distance, δ, suggesting that the repulsion between the micelles is due to the corona behaving as a brush-like layer. A note of caution should be made. The Derjaguin approximation is most applicable when the radius of the curved surfaces is much

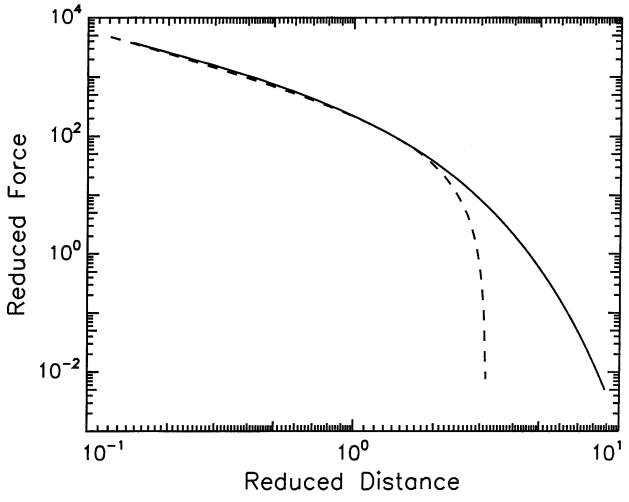

Fig. 13. Reduced force as a function of reduced separation of micelle cores (solid line) compared with the predictions of the model of Patel et al. (dashed line).

larger than the distances between them. Since the micelle core only has a radius of circa 50 Å and the distance at which the repulsion potential becomes finite is not significantly larger than this core radius (~3–4 times core radius), then the Derjaguin may not be applicable. Nonetheless, the reduced force–reduced distance curve obtained from the repulsion potential is remarkably similar to those obtained experimentally from surface forces data for brush layers by Watanabe and Tirrell [43].

5. Conclusions

Diblock copolymers of PS and PEO have been synthesised in all possible variants of deuterium labelling. The copolymers were all of approximately the same composition with a PS weight fraction of ~0.155 ± 0.015 and molecular weights of ~7500 ± 1000 g mol^{-1}. Small angle neutron scattering on aqueous dispersions of these copolymers showed that below concentrations of 1×10^{-2} g ml^{-1} the scattered intensity was due single particle form factors of the micelles. From these data, the micelle morphology was deduced to be spherical with a PS core radius of 56 Å and a PEO corona layer thickness of 125 Å. This latter figure is circa five times the radius of gyration of the equivalent molecular PEO homopolymer in solution. There were circa 170 copolymer molecules in a micelle.

For dispersion with concentrations of 2×10^{-2} g ml^{-1} and above, structure factor scattering became noticeable as a peak in the scattered intensity that moved to higher scattering vector with increasing dispersion concentration. The total scattering was fitted with a combination of form factor and structure factor contributions, but the structure factor contribution could not be reproduced using a hard sphere structure factor expression. A 'softer' Yukawa potential provided excellent fits to the data. From the parameters of the structure factor, osmotic compressibilities of the dispersions have been calculated and correlated with the micelle density in the dispersions. Repulsion potentials calculated from the parameters of the fitted Yukawa potential are not large for the dilute dispersions and we conclude that these dispersions must be subject to considerable thermal fluctuations in the equilibrium separation of the micelles. The repulsive reduced force has also been calculated from these repulsion potentials as a function of the reduced distance between micelles. The form of the curve obtained was very similar to those obtained for the close approach of two brush-like layers using a surface forces apparatus.

Acknowledgements

We thank the Engineering and Physical Sciences Research Council for funding the research programme of which this work forms part and providing a maintenance grant to GJB. The Central Laboratory of the Research Councils is thanked for the provision of the neutron beam facilities at the Rutherford Appleton Laboratory and Dr S.M. King for his assistance with the SANS experiments.

Appendix A. Expression used for structure factor of micellar dispersions

$$S(K) = \frac{1}{1 - 24\eta a(K)}$$

with $K = Q\sigma$ and σ is the diameter of the micelle, η the volume fraction of micelles in the dispersion that is calculated from the number density (n) of micelles using the expression;

$$\eta = \frac{\pi n \sigma^3}{6}$$

and

$$a(K) = \begin{bmatrix} A(\sin K - K\cos K)/K^3 + B[(2/K^2 - 1)K\cos K + 2\sin K - 2/K]/K^3 \\ +\eta A[24/K^3 + 4(1 - 6/K^2)\sin K - (1 - 12/K^2 + 24/K^4)K\cos K]/2K^3 \\ +C(k\cosh k\sin K - K\sinh k\cos K)/K(K^2 + k^2) \\ +F[k\sinh k\sin K - K[\cosh k\cos K - 1)]/K(K^2 + k^2) \\ +F(\cos K - 1)/K^2 \\ -\gamma\exp(-k)(k\sin K + K\cos K)/K(K^2 + k^2) \end{bmatrix}$$

with k and γ the dimensionless screening and coupling constant as defined earlier. The coefficients A, B, C and F are defined in terms of the volume fraction of micelles (η) and the dimensionless screening constant. The detailed expressions for these coefficients and the auxiliary equations used in their definition are given in the paper by Hayter and Penfold [40].

References

[1] Hamley IW. The physics of block copolymers. Oxford: Oxford University Press, 1998.
[2] Araki T, Tran-Cong Q, Shibayama M. Structure and properties of multiphase polymeric materials. New York: Marcel Dekker, 1998.
[3] Bates FS, Schulz MF, Khandpur AK, Forster S, Rosedale JH, Almdal K, Mortensen K. Faraday Discuss 1994;98:7.
[4] Bates FS, Koppi KA, Tirrell M, Almdal K, Mortensen K. Macromolecules 1994;27:5934.
[5] Fredrickson GH, Bates FS. Ann Rev Mater Sci 1996;26:501.
[6] Matsen MW, Bates FS. Macromolecules 1996;29:1091.
[7] Matsen MW, Bates FS. Macromolecules 1996;29:7641.
[8] Matsen MW, Bates FS. J Chem Phys 1997;106:2436.
[9] Ryan AJ, Fairclough JPA, Hamley IW, Mai S-M, Booth C. Macromolecules 1997;30:1723.
[10] Plestil J, Baldrian J. Makromol Chem 1973;174:183.
[11] Plestil J, Baldrian J. Makromol Chem 1975;176:2009.
[12] Shibayama M, Hashimoto T, Kawai H. Macromolecules 1983;16:16.
[13] Shibayama M, Hashimoto T, Kawai H. Macromolecules 1983;16:1434.
[14] Shibyama M, Hashimoto T, Hasegawa H, Kawai H. Macromolecules 1983;16:1427.
[15] Fetters LJ, Richards RW, Thomas EL. Polymer 1987;28:2252.
[16] Alexander S. J Phys (Paris) 1977;38:977.
[17] de Gennes PG. Macromolecules 1980;13:1069–75.
[18] Dan N, Tirrell M. Macromolecules 1992;25:2891.
[19] Daoud M, Cotton JP. J Phys (Paris) 1982;43:531.
[20] Gast AP. Langmuir 1996;12:4060.
[21] McConnell GA, Lin EK, Gast AP, Huang JS, Lin MY, Smith SD. Faraday Discuss 1994;98:121.
[22] McConnell GA, Gast AP. Macromolecules 1997;30:435.
[23] Jada A, Hurtrez G, Siffert B, Riess G. Makromol Chem Phys 1996;197:3697.
[24] Mortensen K, Brown W, Almdal K, Alami E, Jada A. Langmuir 1997;13:3635.
[25] Dewhurst PF, Lovell MR, Jones JL, Richards RW, Webster JRP. Macromolecules 1998;31:7851.
[26] Alexander M, Richards RW. J Phys Chem B 2000;104:9179.
[27] Burchard W. In: Happey F, editor. Light scattering techniques, Vol. 1. London: Academic Press, 1978.
[28] King SM. In: Pethrick RA, Dawkins JV, editors. Small-angle neutron scattering, Chichester: Wiley, 1999.
[29] Ottewill RH, Goodwin J. editors. London: Royal Society of Chemistry, 1986.
[30] Egelstaff P. An introduction to the liquid state. 2nd ed. Oxford: Oxford University Press, 1992.
[31] Guinier A, Fournet G. Small-angle scattering of X-rays. New York: Wiley, 1955.
[32] Percus JK, Yevick GJ. Phys Rev 1958;110:1.
[33] Ashcroft NW, Lekner J. Phys Rev 1966;145:83.
[34] Ornstein LS, Zernike F. Proc Acad Sci Amsterdam 1914;17:793.
[35] Kinning DJ, Thomas EL. Macromolecules 1984;17:1712.
[36] Alexander K, Cebula DJ, Goodwin JW, Ottewill RH, Parentich A. Colloids Surf 1983;7:233.
[37] Jialanella CL, Firer EM, Piirma I. J Polym Sci, Pt A, Polym Chem 1992;30:1925.
[38] Kawaguchi S, Imai G, Suzuki J, Miyahara A, Kitano T, Ito K. Polymer 1997;38:2885.
[39] Hansen J-P, Hayter JB. Mol Phys 1982;46:651.
[40] Hayter JB, Penfold J. Mol Phys 1981;42:109.
[41] Hayter JB, Hansen J-P. The structure factor of charged colloidal dispersions at any density, Institut Laue-Langevin, 1982.
[42] Patel S, Tirrell M, Hadzioannou G. Colloids Surf 1988;31:157.
[43] Watanabe H, Tirrell M. Macromolecules 1993;26:6455.
[44] Derjaguin BV. Kolloid Z 1934;69:155.